

Unusual Fish Assemblages Associated with Environmental Changes in the East China Sea in February and March 2017

Wenxiang Ding, Caiyun Zhang *, Jianyu Hu and Shaoping Shang

State Key Laboratory of Marine Environmental Science, Key Laboratory of Underwater Acoustic Communication and Marine Information Technology Ministry of Education, College of Ocean and Earth Sciences, Xiamen University, Xiamen 361102, China; wenxiangding2015@163.com (W.D.); hujiy@xmu.edu.cn (J.H.); spshang@xmu.edu.cn (S.S.)

* Correspondence: cyzhang@xmu.edu.cn

Abstract: Two large fish assemblages were recorded in the overwintering fishing grounds of the East China Sea in February and March 2017. In this study, available time series of satellite-derived sea surface temperature, wind, chlorophyll *a*, and reanalysis data were used to explore the relationships between the observed large fish aggregations and environmental factors. The bottom waters of the fishing grounds were abnormally warm in winter 2017, and then experienced significant cooling due to the eastward movement of the Yellow Sea Cold Current, which was driven by the increased northwesterly wind from January to mid-March 2017. Fishing areas in the affected region, including No. 1891, which was abnormally warm, and No. 1592, which had a strong thermal front and high chlorophyll *a* concentration, might have provided suitable environments for the warm-temperature fish, resulting in the observed large fish assemblages. The abnormal temperature changes between winter and early spring 2017 may have been associated with changes in local ocean circulation.

Citation: Ding, W.; Zhang, C.; Hu, J.; Shang, S. Unusual Fish Assemblages Associated with Environmental Changes in the East China Sea in February and March 2017. *Remote Sens.* **2021**, *13*, 1768. <https://doi.org/10.3390/rs13091768>

Academic Editors: Antony Liu and Jorge Vazquez

Received: 2 March 2021
Accepted: 29 April 2021
Published: 1 May 2021

Publisher's Note: MDPI stays neutral with regard to jurisdictional claims in published maps and institutional affiliations.



Copyright: © 2021 by the author. Licensee MDPI, Basel, Switzerland. This article is an open access article distributed under the terms and conditions of the Creative Commons Attribution (CC BY) license (<http://creativecommons.org/licenses/by/4.0/>).

Keywords: fish assemblage; temperature; environmental change; Yellow Sea Coastal Current; East China Sea

1. Introduction

Changes in fishery resources are not only associated with increased anthropogenic fishing pressure, but are also closely related to fluctuations in marine environmental factors, such as winds, sea surface temperatures (SST), and ocean currents [1–3]. Of these, temperature has the most significant effect on fish activity [4]. Changes in temperature directly or indirectly affect fish migration behaviors, growth, and habitat distributions [5–7]. Eveson et al. [8] demonstrated that water temperature is the environmental variable most commonly used to forecast tuna fishing grounds. The strong relationships between temperature and fish abundance are well documented [9]. In addition, several studies investigated the effects of abrupt changes in temperature on fishing grounds and fishery resources, e.g., [4,10]. For example, some fish species shifted northward during the 2012 ocean heat wave in the Northwest Atlantic [4], while a cold event in 2008 contributed to a massive fish die-off near the Penghu Island, Taiwan [10].

The East China Sea (ECS) is a marginal sea in the western Pacific Ocean that has a vast shallow continental shelf (Figure 1). The Yangtze River carries a large volume of terrestrial material into the ECS, and the southeastern ECS is strongly affected by the warm Kuroshio current [11,12]. The ECS circulation is influenced by the East Asian monsoon: Northerly winds prevail in winter, while southerly winds prevail in summer [13]. The primary currents affecting the ECS include the Kuroshio, Taiwan Warm Current (TWWC), Yellow Sea Warm Current (YSWC), Yellow Sea Coastal Current (YSCC), and Zhe-Min Coastal Current [1,14]. Interactions among bottom topography, large freshwater

discharge, monsoon winds, and the Kuroshio intrusion led to the development of particular circulation regimes and distinct water masses [1]. Ocean parameters, such as temperature and salinity, may change abruptly between water masses [15]. Fronts, which are defined as boundaries between water masses, are generally characterized by strong mixing and increased bioproductivity [16–18]. Thus, frontal zones often coincide with fishery grounds in the ECS [19].

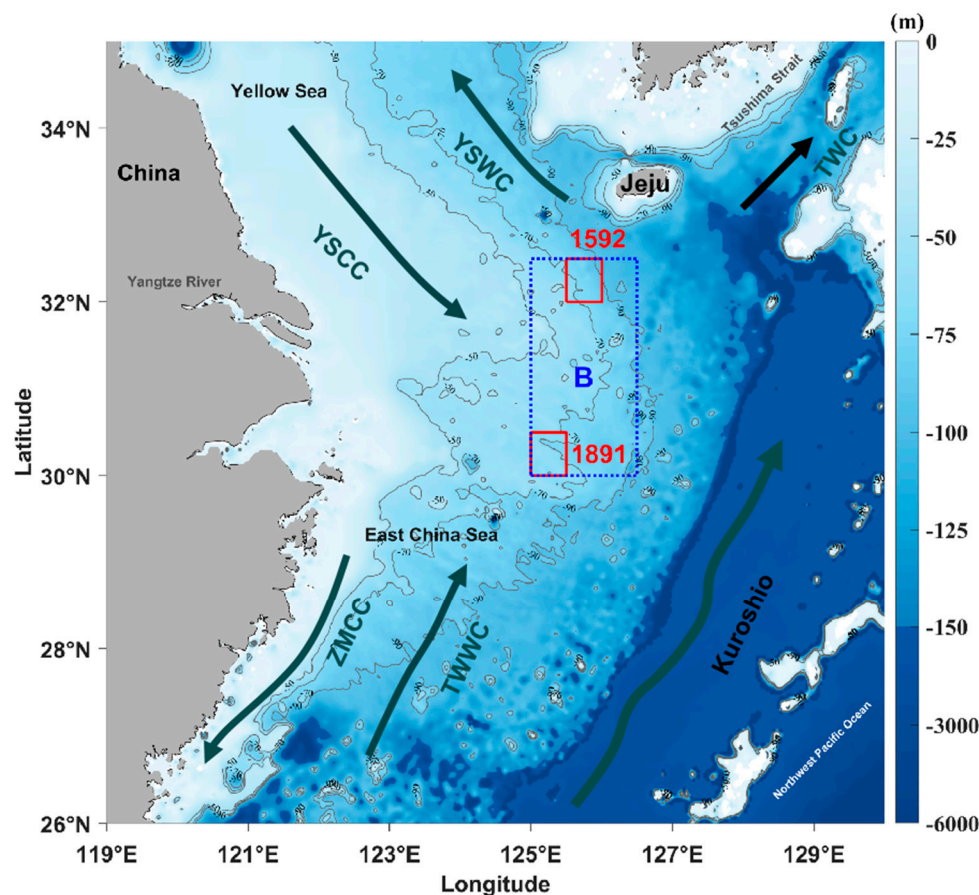


Figure 1. Map showing the study area and water circulation in winter. The two red boxes outline the two fishing areas (Nos. 1592 and 1891). Area B, which includes Nos. 1592 and 1891, is boxed by blue dotted lines. The light gray lines represent isobaths. The bathymetric data were obtained from the General Bathymetric Chart of the Oceans (GEBCO_2020) grid data from the British Oceanographic Data Centre. TWWC: Taiwan Warm Current; ZMCC: Zhe-Min Coastal Current; YSCC: Yellow Sea Coastal Current; YSWC: Yellow Sea Warm Current; TWC: Tsushima Warm Current.

Being one of the most important fishing grounds in the west Pacific, the ECS is biologically diverse and rich in fishery resources, with over 700 recorded species of fish, more than 100 species of crustaceans, and 69 species of cephalopods [20–22]. All fish species are considered inshore, offshore, or migratory [23]. Migratory species include the small yellow croaker (*Larimichthys polyactis*), hairtail, red seabream, and Pacific herring [23]. These species spawn and mature in shallow nearshore waters, then migrate for food and overwintering far offshore [23]. Previous studies show that the abundances and spatial distributions of fishery resources in the ECS are closely related to variations in marine environmental variables [24–26]. For example, due to the influence of various currents and water masses, primary productivity in the ECS is high during the summer [27]. Thus, the ECS is an important spawning and nursery ground for commercially valuable fish such as the small yellow croaker, hairtail, pomfret, and white Chinese croaker [26].

ECS fisheries began to be heavily exploited in the 1980s [28,29], and the biodiversity and abundance of commercial fish species decreased significantly since that time [30]. In the 1990s, the abundance of large-sized, commercially high-value fish species, such as hairtail, small yellow croaker, and silver pomfret, declined to less than 50% of levels in the 1980s, and low-value species began to dominate the catch [29,31]. In addition, although fishing power increased by a factor of 7.6 between the 1960s and the 1990s, the catch per unit effort in the ECS declined by a factor of 3 over the same period [23,32].

In late February 2017, a large number of small yellow croaker (*L. polyactis*) appeared at the surface of fishing area No. 1891 in the ECS (Figure 2a). Fishermen caught more than 9000 kg of *L. polyactis* in about two hours (available online: http://slide.news.sina.com.cn/s/slide_1_2841_108157.html#p=1, accessed on 2 March 2021). Two weeks later, in mid-March 2017, fishermen caught more than 90,000 kg of *Collichthys sp.* and *L. polyactis* near fishing area No. 1592 in about ten days (Figure 2b) (available online: https://www.sohu.com/a/128766304_115864, accessed on 2 March 2021). Large fish catches over short periods such as these are very rare in the ECS, especially as fishery resources are currently reduced due to overfishing. Although some previous studies explored long-term variations in fishery resources and the relationship between these variations and climate change [33–36], investigations of the environmental factors associated with the sudden appearance of abundant fish assemblages in the ECS are limited.



Figure 2. Fishermen catching large quantities of fish in the ECS. *Larimichthys polyactis* caught in fishing area No. 1891 in late-February 2017 (a, available online: http://slide.news.sina.com.cn/s/slide_1_2841_108157.html#p=1, accessed on 2 March 2021); *Collichthys sp.* and *L. polyactis* caught in fishing area No. 1592 in mid-March 2017 (b, available online: https://www.sohu.com/a/128766304_115864, accessed on 2 March 2021).

Therefore, to investigate the drivers of the large fish assemblages recorded between February and March 2017, we utilized time series data for satellite-derived sea surface temperature (SST), wind, and Chl *a* concentration, and we used reanalyzed data including data covering temperature and geostrophic currents to investigate variations in marine environmental factors across the fishing grounds, particularly Nos. 1891 and 1592. This study aimed to explore possible mechanisms associated with the large fish accumulations

observed in February and March 2017. Usually, large fish assemblages are rare and difficult to predict. However, an improved understanding of the complex relationships among environmental factors in marine ecosystems will help to clarify the responses of fishery resources to marine environmental change, and will inform the development of fishery policies that anticipate future changes in resource availability due to abrupt shifts in marine conditions.

2. Materials and Methods

2.1. Satellite Data and Processing

Daily and monthly global Operational Sea Surface Temperature and Sea Ice Analysis (OSTIA) data from 2011 to 2019 were obtained from the European Copernicus program (<http://marine.copernicus.eu>, accessed on 2 March 2021), and Advanced Scatterometer (ASCAT)-derived wind-speed and wind-direction data for the same period were obtained from Remote Sensing Systems (<http://www.remss.com>, accessed on 2 March 2021). The spatial resolution of the OSTIA global sea surface temperature (SST) data is 5 km, and that of the ASCAT-derived wind data is 25 km. Monthly Chl *a* data from the Moderate Resolution Imaging Spectroradiometer (MODIS)/Aqua were obtained from the NASA Goddard Space Flight Center (<https://oceancolor.gsfc.nasa.gov>, accessed on 2 March 2021) and have a spatial resolution of 4 km. Daily Chl *a* concentration data, derived from geostationary satellite Himawari-8, were obtained from the P-Tree System (Japan Aerospace Exploration Agency, <https://www.eorc.jaxa.jp/ptree/index.html>, accessed on 2 March 2021) and have a spatial resolution of 5 km.

Temporal changes in the main marine environmental factors in fishing areas No. 1592 (125.5°E–126.0°E, 32°N–32.5°N) and No. 1891 (125.0°E–125.5°E, 30°N–30.5°N; Figure 1) were analyzed, as the abnormal fish assemblages of 2017 were observed in these areas. We also established a larger study site surrounding fishing areas Nos. 1592 and 1891 (area B; 125°E–126.5°E, 30°N–32.5°N) in order to investigate the main environmental parameters of the overwintering fishing grounds.

Gradient methods are commonly used to recognize and define oceanic fronts. The amplitude $grad(i, j)$ of the SST gradient was computed at each grid point (i, j) in the ECS using the central difference method of Wall et al. [37] as follows:

$$grad(i, j) = \sqrt{\left(\frac{SST_{i+1,j} - SST_{i-1,j}}{2\Delta x}\right)^2 + \left(\frac{SST_{i,j+1} - SST_{i,j-1}}{2\Delta y}\right)^2} \quad (1)$$

where Δx and Δy are the distances in kilometers between pairs of neighboring grid points in the east-west direction and the north-south direction, respectively.

Here, we defined thermal fronts as those where the SST gradient was ≥ 0.025 °C/km. In this way, the weak front at the southern edge of the YSCC was manifested. The frontal intensity was then calculated as the average SST gradient of the pixels with gradients greater than the threshold. We also calculated frontal intensity using other frontal thresholds (e.g., gradient thresholds of ≥ 0.01 , ≥ 0.015 , and ≥ 0.02 °C/km) and compared our results with those generated using a gradient threshold of ≥ 0.025 °C/km (Figure 3). We found no significant differences among daily frontal intensities calculated based on different thresholds for fishing areas No. 1891 and 1592 between January and May 2017 (Figure 3). The correlation coefficient (R^2) was >0.74 for fishing area No. 1891 and >0.96 for fishing area No. 1592.

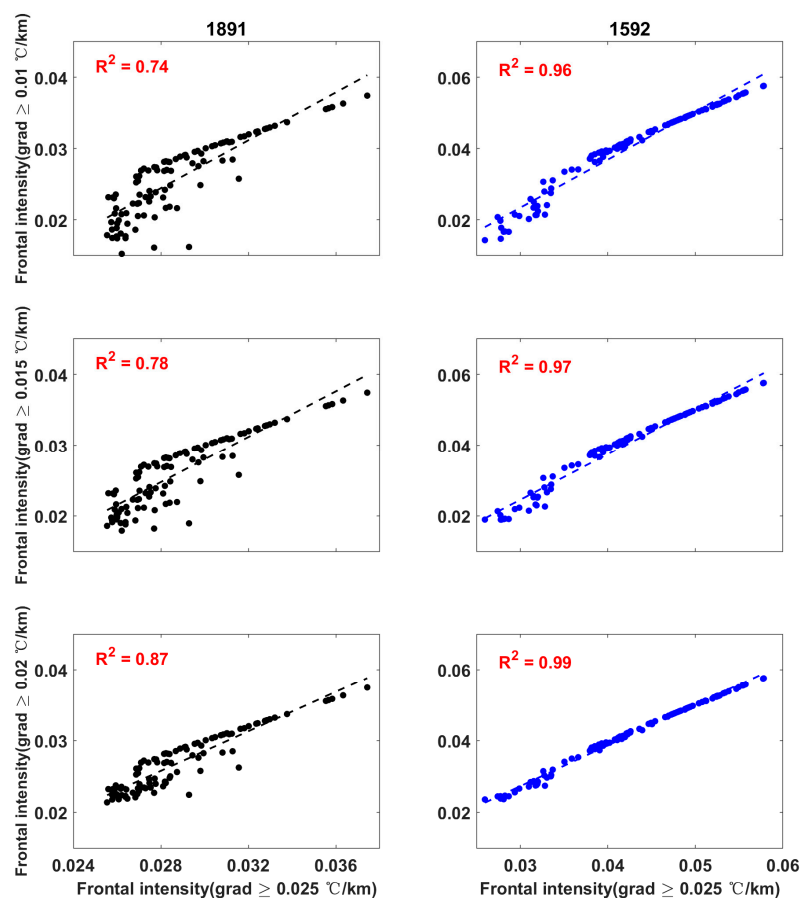


Figure 3. Daily frontal intensities from January to May 2017 calculated using different frontal thresholds for fishing areas No. 1891 (left panels) and No. 1592 (right panels).

Nighttime light remote sensing data were previously shown to be an effective proxy with which to monitor fishing activity and evaluate fishery resources [38,39]. Waluda et al. [40] used satellite-derived nighttime lights to show that fish catch was positively correlated with estimated fishing extent. Indeed, light intensity at night affects fish activity levels and aggregation [41,42]. Because monthly fish catch data at the study sites are not available, we used nighttime light intensity to approximate the temporal changes in fishery activity levels. Higher light intensities might imply increases in fishing effort or fish abundance. The monthly average radiance composite images derived from the Visible Infrared Imaging Radiometer Suite (VIIRS) Day/Night Band (DNB) for February and March from 2013 to 2019 were obtained from the Earth Observations Group (<https://payneinstitute.mines.edu/eog/nighttime-lights/>, accessed on 2 March 2021), with a spatial resolution of 15 arc-seconds (~500 m). DNB radiance data affected by stray light, lightning, lunar illumination, and cloud cover are excluded from the DNB datasets before averaging [43]. We used the average monthly radiance data greater than zero in area B to analyze temporal changes in nighttime light intensity.

2.2. Temperature and Geostrophic Currents from ARMOR3D

The Multi Observation Global Ocean ARMOR3D L4 multi-year reprocessed (REP) weekly data from 2011 to 2019 were obtained from the E.U. Copernicus Marine Service (<http://marine.copernicus.eu>, accessed on 2 March 2021). The product used in this study was MULTIOBS_GLO_PHY_TSUV_3D_MYNRT_015_012. The ARMOR3D product consists of global 3D temperature, salinity, geopotential height, geostrophic currents, and 2D mixed layer depth defined on a $1/4^\circ$ regular grid, from the surface down to a depth of 5500

m [44,45]. The temperature and salinity observation-based product uses statistical methods to combine remote sensing observations (sea level anomaly and SST) with in situ vertical profiles of temperature and salinity (derived mainly from Argo floats but also from other sources including Conductivity-Temperature-Depth (CTDs) and eXpandable-Bathy-Thermograph (XBTs)) [45]. The global 3D geostrophic circulation was estimated by merging altimetric data and a synthetic 3D thermohaline field using the thermal wind equation with the reference level set at the surface [44].

3. Results

3.1. Temperature

The spatial distribution of average SST in the ECS from February to March clearly showed a cold-water tongue, represented by a 12.5 °C isotherm, extending southeastward from the Yellow Sea (Figure 4). Fishing areas Nos. 1891 and 1592 were located at the edge of this cold-water tongue. Unlike the 12.5 °C isotherm observed each year from 2011 to 2019 (but excluding 2011 and 2017), the 12.5 °C isotherm of 2017 shifted northwards or eastwards (Figure 4).

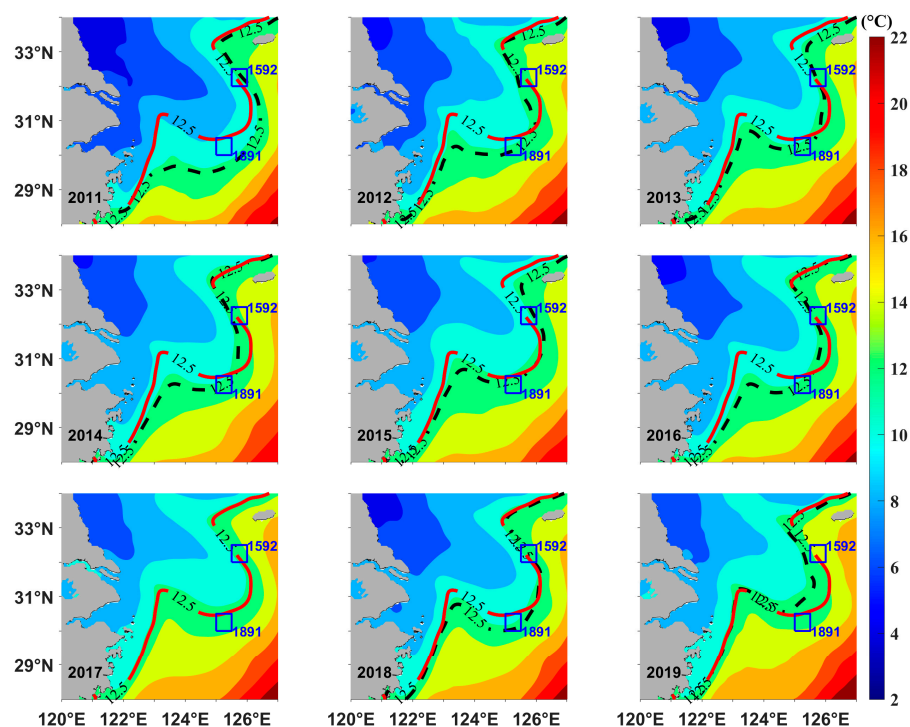


Figure 4. The spatial distributions of average OSTIA SST in February and March in the East China Sea from 2011 to 2019. The overlaid solid red line represents the 12.5 °C isotherm based on the average SST from February to March in 2017, while the dashed black line represents the 12.5 °C isotherm based on average SST from February to March in the year indicated.

Daily variations in SST between January and April from 2011 to 2019 indicated that relatively high SST took place early in January in both fishing areas Nos. 1891 and 1592. Then, the SSTs decreased until mid- or late-March (Figure 5). The SST of No.1891 was warmer in 2017 than in other years on the same days before mid-March. For No. 1592, warm SST appeared in early January, and it was warmer than the SSTs of other years excepting 2019. After that, the SST decreased and was <12 °C in mid-March 2017 (Figure 5).

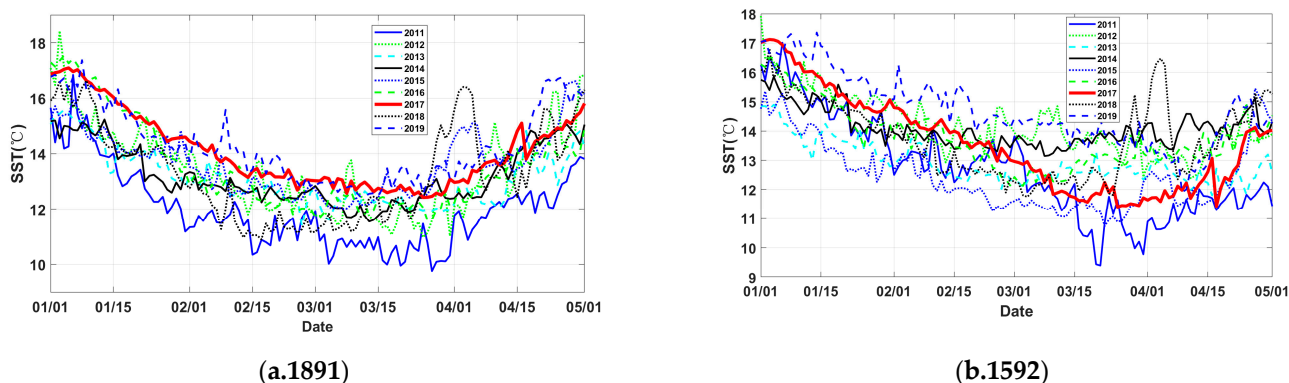


Figure 5. Daily SST between January and April 2011–2019 for (a) fishing area No. 1891 and (b) fishing area No. 1592. The thickened red lines correspond to 2017.

The vertical distributions of temperature derived from ARMOR3D for area B between 2011 and 2019 are shown in Figure 6. The upper 50 m of the water column in area B was relatively cold and vertically mixed; the bottom layer was warmer, possibly due to the influence of the TWCC [46]. Compared with other years, the bottom layer (60–80 m) in early January 2017 was relatively warm ($>18\text{ }^{\circ}\text{C}$), warmer than any other years except for 2016 and 2019 (Figures 6 and 7). Then, water temperature decreased, and relatively cold water ($<14\text{ }^{\circ}\text{C}$) appeared in March 2017 (Figure 6). We calculated the differences in water temperatures between the week with the coldest average water temperature (the 11th week, March 12–18) and the week with the warmest average temperature (the 1st week, January 1–7) for the upper layer (0–20 m) and the bottom layer (60–80 m) (Figure 7). We found that the magnitude of cooling in area B from early January to mid-March 2017 was generally greater than that in any of the other nine years. This was especially dramatic in the bottom layer, the temperature of which decreased by $>4\text{ }^{\circ}\text{C}$ between early January to mid-March 2017, a greater decrease than that in any other year (Figure 7).

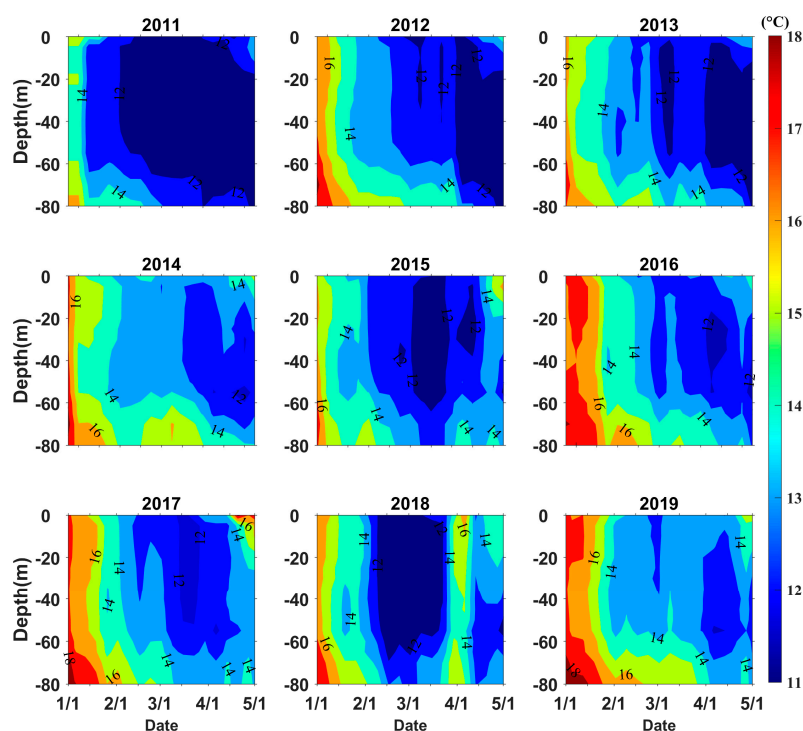


Figure 6. Vertical distributions of temperature between January and April 2011–2019 for area B.

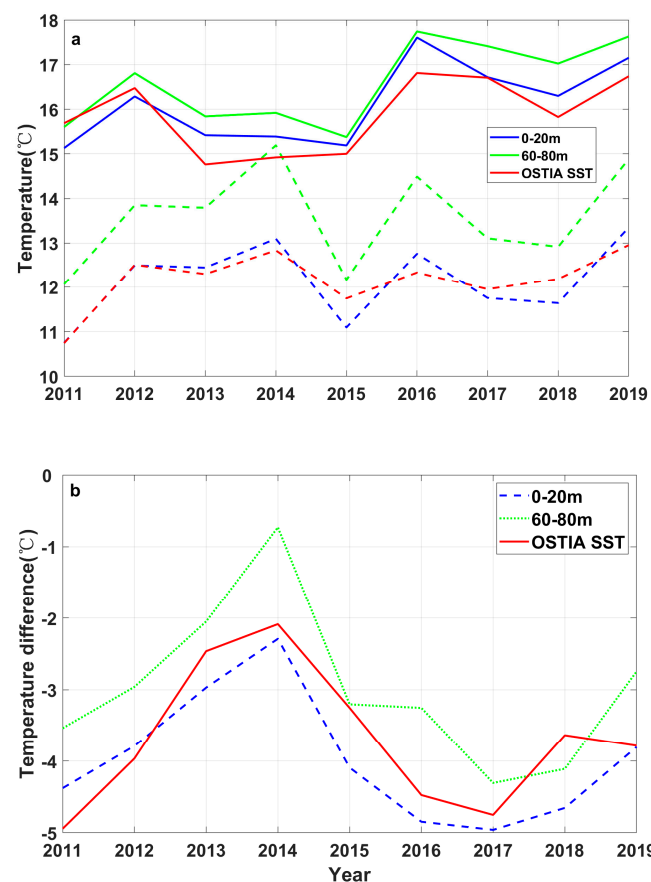


Figure 7. Temperatures in the 1st week (solid lines) and 11th week (dashed lines) in the upper layer (0–20 m) and the bottom layer (60–80 m) in area B. Both temperatures are graphed in (a); differences between the 1st and 11th week are shown in (b). The OSITA SSTs are superimposed for comparison.

3.2. Thermal Fronts

The spatial distribution of the SST gradient in the ECS is shown in Figure 8. A high SST gradient was particularly noticeable at the northern edge of the cold-water tongue, where the cold YSCC meets the warm YSWC. Fishing area No. 1592 is located inside the northern strong thermal front, and fishing area No. 1891 is located at the edge of the southern weak thermal front (Figure 8a). The frontal intensity in the fishing area No. 1592 was stronger than the multi-year average, while the intensity of the thermal front in most of fishing area No. 1891 was weaker than in normal years (Figure 8b).

Daily changes in frontal intensity between 1 January 2017 and 1 May 2017 indicate that the frontal intensity in fishing area No. 1891 was weaker than that in fishing area No. 1592 (Figure 9). The strongest frontal intensity in fishing area No. 1891 appeared in late January. Frontal intensity remained relatively strong through mid-February and became relatively weak in March. The strongest frontal intensity in fishing area No. 1592 appeared in mid-February, about one month later than that in fishing area No. 1891. Thus, in neither area did the appearance of the unusually large fish assemblage exactly coincide with the peak of frontal intensity. However, the large fish assemblage did appear in fishing area No. 1592 at a point when frontal intensity was relatively strong (Figure 9). Compared with multi-year average, the frontal intensity in fishing area No. 1891 was weaker on most days in February and March 2017. However, the frontal intensity in fishing area No. 1592 was higher than average between January and mid-March 2017 (Figure 9).

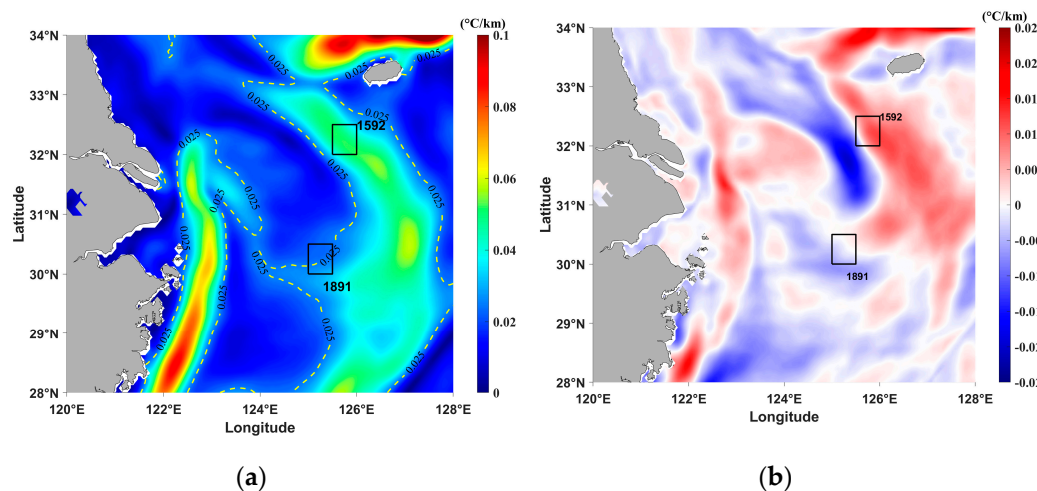


Figure 8. (a) The spatial distribution of the average SST gradient and (b) the gradient anomaly during February and March 2017. The gradient anomaly was obtained by subtracting the average gradients for February and March 2011–2019 from the gradients for February and March 2017.

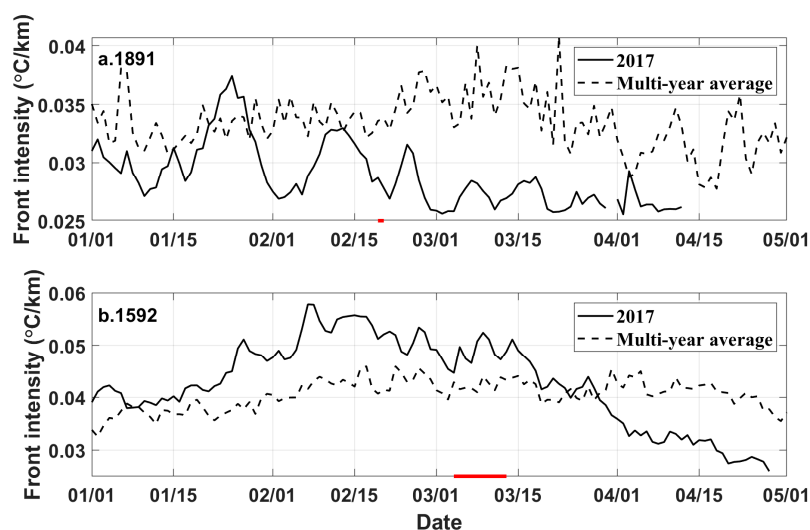


Figure 9. (a) Daily fluctuations in frontal intensity for fishing area No. 1891 and (b) fishing area No. 1592 from January to April 2017. The solid and dashed lines indicate the frontal intensity in 2017 and the average frontal intensity in 2011–2019, respectively. The bold red lines on each x-axis indicate the time periods at which the large fish assemblages were observed in each area (as shown Figure 2).

3.3. Chl *a*

Analysis of the spatial distribution of MODIS Chl *a* concentration in February and March 2017 showed that nearshore Chl *a* was greater than offshore Chl *a* (Figure 10a). Chl *a* concentrations were greater than 1.0 mg/m^3 in both fishing areas (Nos. 1891 and 1592). In 2017, Chl *a* levels greater than the multi-year average mostly occurred in or near thermal fronts (Figure 10b), and these locations also had stronger than average frontal intensities (Figure 8b). Indeed, the Chl *a* concentration in fishing area No. 1592 was 0.21 mg/m^3 (11.9%) higher than the multi-year average.

Because several datapoints in the daily Himawari-8-derived Chl *a* dataset for fishing areas Nos. 1891 and 1592 are missing due to bad weather or cloud cover, we used the daily changes in Chl *a* concentration in area B as a whole (including both fishing areas; Figure

10c). Chl *a* concentrations were relatively high from early February to mid-March, consistent with the appearance of relatively intense fronts (Figure 9).

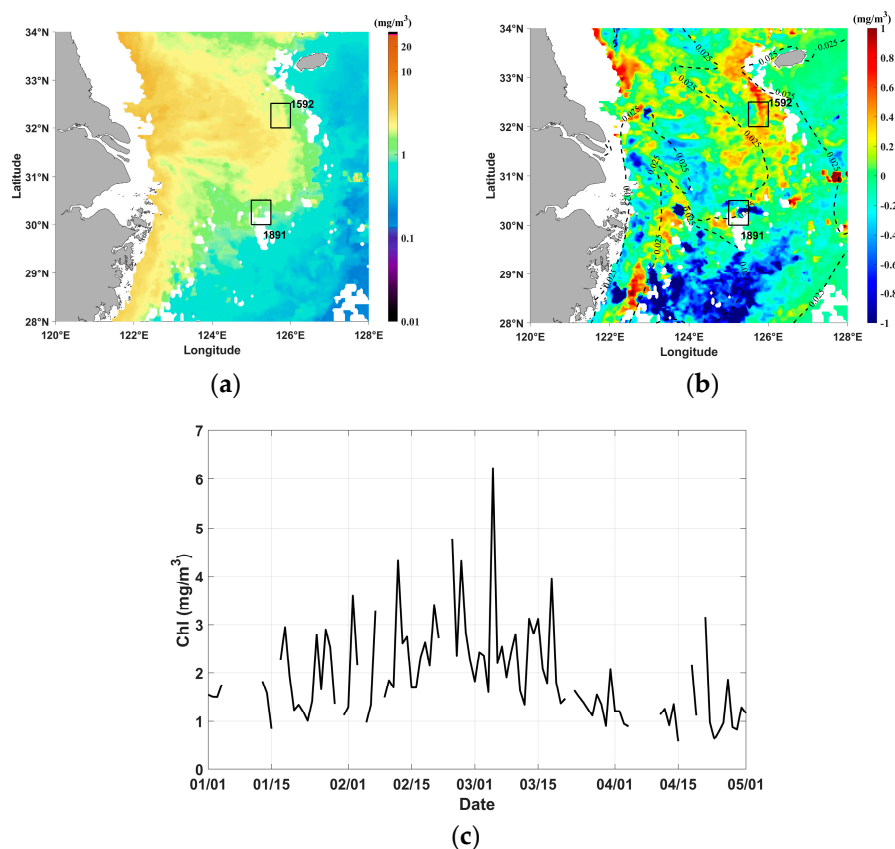


Figure 10. (a) The spatial distribution of average MODIS-derived Chl *a* concentrations and (b) Chl *a* anomalies in area B, overlaid with an SST gradient of 0.025 °C/km in February and March 2017. (c) Daily changes in Himawari-8-derived Chl *a* concentrations in area B. Chl *a* anomaly data were calculated by subtracting the average Chl *a* concentration in February and March 2011–2019 from the Chl *a* concentration in February and March 2017.

3.4. Wind

Northerly winds prevailed in the ECS during February and March 2017 (Figure 11a). The polar wind chart indicates that the wind field in 2017 was mainly northerly and northwesterly, in contrast to the multi-year average wind field, which was dominated by northerly and northeasterly winds (Figure 11b). The frequencies of northerly and northwesterly winds in February and March 2017 were greater than the multi-year average, while the frequencies of northeasterly winds were significantly lower. Furthermore, the speeds of northerly and northwesterly winds in February and March 2017 were significantly stronger than the multi-year average, while the northeasterly winds were weaker (Figure 11b).

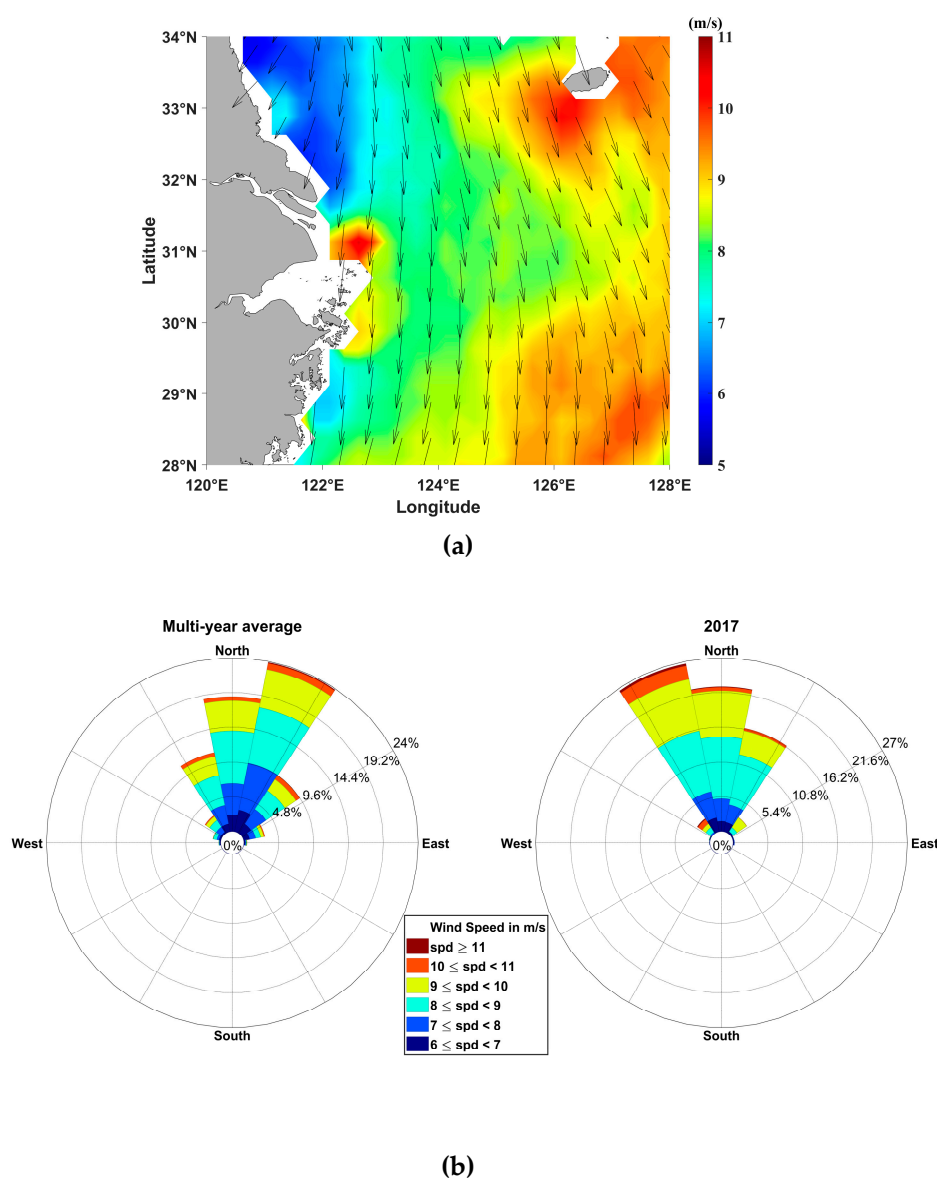


Figure 11. (a) The spatial distribution of the average wind field in February and March 2017. The color represents wind speed, and the black arrows indicate wind direction. (b) The polar wind chart showing the multi-year average wind for 2011–2019 (left panel) and the average wind in February and March 2017 (right panel).

4. Discussion

During February and March 2017, large fish assemblages were observed in fishing areas Nos. 1891 and 1592 (Figure 2). We used monthly average nighttime light radiance data to demonstrate that fish abundance was also high in other locations in area B (Figure 12a). Nighttime light radiance in area B was high in 2017 and 2018 (Figure 12a). The average radiance in February and March 2017 was 38% higher than that of 2013–2016. High radiance levels correspond to higher light intensities, indicating that greater fishing fleets and fish abundance were at sea [40]. Indeed, it was previously reported that many fisheries worldwide use artificial light to attract pelagic fish and increase fish catches, e.g., [41,47]. Our results suggested that there might have been a considerable number of fishing fleets operating near the fishing grounds of area B due to the relative abundance of fish during February and March 2017 (Figure 12a).

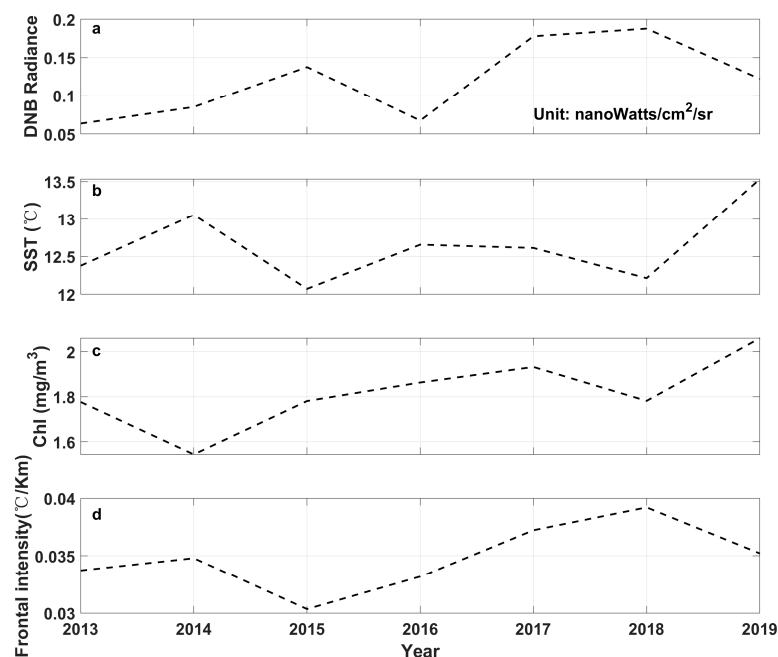


Figure 12. (a) Average DNB radiance, (b) SST, (c) Chl *a*, and (d) frontal intensity in February and March 2013–2019 in area B (the area outlined with a dashed blue line in Figure 1).

L. polyactis and *Collichthys sp.*, which are economically important fishery species in China, are warm-temperate demersal fish [48,49]. Generally, the spawning grounds of these fish are located on the inner shelf of the ECS or its estuaries [50]. Due to the south-eastward intrusion of the cold YSCC in the winter, the nearshore environment becomes unsuitable for the growth of these species; both species thus migrate to warm offshore areas and overwinter at depths of 40–80 m [51–53]. Previous studies showed that the main winter fishing grounds in the ECS are located at the southern shelf area, where the YSCC and TWWC meet, or at the eastern slope area, where the YSCC and YSWC meet [50]. The two fishing areas examined in this study, Nos. 1891 and 1592, are located in these mixed waters (Figure 1). These fishing grounds are influenced by various different water masses and consequently have strong temperature and salinity gradients [15]. These fishing grounds also include areas with high abundances of small- and medium-sized copepods, which provide a rich food source for *L. polyactis* and *Collichthys sp.* [54]. Therefore, *L. polyactis* and *Collichthys sp.* tend to migrate and gather in these fishing areas for the winter.

Environmental changes strongly affect the paths, compositions, and durations of fish migrations for feeding or overwintering [55–57]. In January 2017, the bottom water became relatively warm (>18 °C). The water temperature in this layer then decreased due to the eastward movement of the cold YSCC. The decrease in the temperature of the bottom layer was especially dramatic in 2017 (Figure 7). Liu et al. [58] indicated that *L. polyactis* tolerate a wide range of temperatures (6–26 °C). However, as both *L. polyactis* and *Collichthys sp.* are warm-temperate demersal fish, they might tend to migrate to warmer water [50]. Indeed, *L. polyactis* and *Collichthys sp.* may not have been able to tolerate the continuous cooling of the bottom layer in February and March 2017, and these fish may have attempted to migrate to the surrounding warm water.

Fishing areas Nos. 1891 and 1592 are located at the edge of the cold-water tongue, and are warmer than the surrounding water that is influenced by the YSCC (Figure 4). Fishing area No. 1891 was warmer than average during January and March 2017 (Figure 5a), although frontal intensity was weak, and Chl *a* concentrations were not high (Figures 8 and 10). Several studies suggested that fish abundance increases with temperature, e.g., [9,59,60]. Therefore, the warmth of fishing area No. 1891 in February 2017 might have

provided favorable conditions for warm-temperature fish, causing the observed large aggregation of fish in this fishing area (Figure 2). However, the factors leading to the large aggregation of fish on the sea surface in fishing area No. 1891 remain unclear due to limited data. Additional observations, combined with fish behavior analyses, are necessary to understand better the factors that generated this aggregation at the surface.

In contrast to fishing area No. 1891, fishing area No. 1592 had stronger fronts (Figures 8 and 9) and higher Chl *a* concentrations (Figure 10) in 2017 as compared to other years. Usually, a strong front is characterized by abundant nutrients and high primary productivity [61–64], which provides a suitable habitat for fish [48,65]. Figure 12 shows the inter-annual variation in nighttime light intensity, average SST, front intensity, and Chl *a* concentrations for area B over the period 2013–2019. The two years with the greater light intensity (2017 and 2018) also seem to have high frontal intensity (Figure 12a,d). These results further suggested that fishing grounds with high frontal intensity attracted more fish schools. Consequently, fish abundance was high in these frontal areas, and more fishing boats were present.

Fishery resources in the ECS have been gradually increasing as a result of recent moratoriums on summertime fishing [49]. As fishing grounds recover, large fish assemblages may reappear in the ECS. It is possible that the particular environmental conditions identified in winter and spring 2017, which provided a suitable environment for migratory fish and which may have played an important role in the large fish aggregations of that year, were also present in other years. These conditions included the relatively warm temperature of the bottom layer in January (Figure 6), followed by a significant cooling of the bottom layer between January and March (Figures 6 and 7), while the surrounding waters remained warm; these conditions also included the observed strong frontal intensity and high Chl *a* concentrations. Long-term time series of multi-disciplinary data, including historical catch data, should be collected to investigate the complex relationships between environmental change and variations in fishery resources further.

Numerous studies previously showed that increases in ECS temperatures are associated with global warming [66,67], and average winter SST in the ECS has increased an average of ~ 0.3 °C/decade, which far exceeds the globally averaged rate of ocean surface warming [68]. Indeed, the ECS experienced record-high temperatures in the winter months of 2017 [69], which was consistent with the high temperatures recorded in January 2017 (Figures 5 and 6).

The significant cooling from January to mid-March 2017 might be linked to the eastward movement of cold YSCC (Figures 4 and 13a). Circulation in the ECS and the Yellow Sea is controlled by the East Asian monsoon [70,71]. As shown in Figure 13a, the Kuroshio, TWC, and TWWC have greater northward velocities than other surrounding currents. The frequent and strong northerly and westerly winds (Figure 11) in February and March 2017 enhanced the YSCC (Figure 13b), which might have driven more cold water from the Yellow Sea into the northern ECS, causing the cold-water tongue of the YSCC to move further eastward in February and March (Figures 4 and 13b). At the same time, the warm TWWC in the south moved abnormally northward (Figure 13b), raising the SST of fishing area No. 1891 above the multi-year average (Figures 4 and 5). The strengthened YSCC reduced SSTs, increasing the temperature difference between the YSCC and the YSWC. This increased frontal intensity between the cold and warm water masses (Figure 8) led to an increase in Chl *a* concentrations (Figure 10). As demonstrated by Weisberg et al. [72], ocean circulation unites nutrients with light, fueling primary productivity and higher trophic level interactions. Thus, ocean currents may play an important role in the regulation of phytoplankton growth and fishery resources.

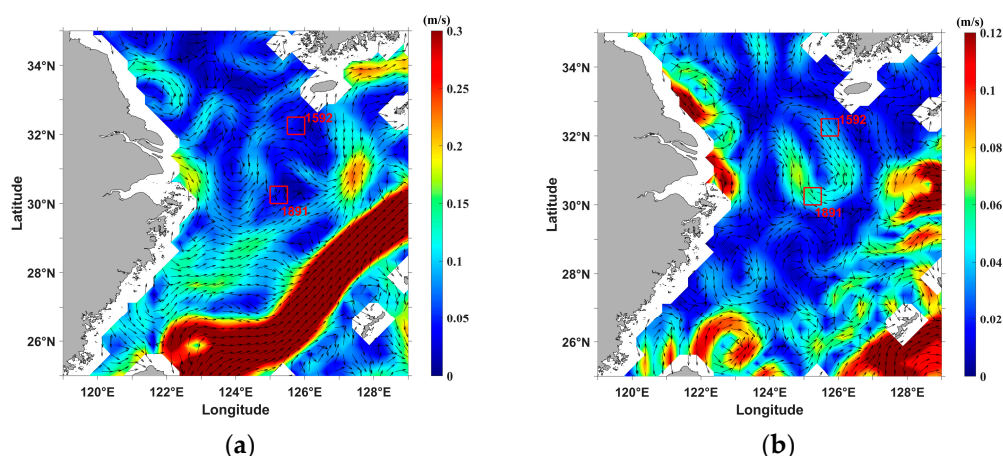


Figure 13. (a) The distribution of average sea surface currents (SSCs) and (b) SSC anomalies in February and March 2017. Colors correspond to current speed, while arrows indicate current direction. SSC anomaly data were calculated by subtracting the average SSC during February and March 2011–2019 from the SSC in February and March 2017.

Over recent decades, ocean temperatures increased steadily due to climate change, and these increases strongly impacted the marine ecosystem [73–75]. The ECS was previously identified as a critical area of significant ocean warming, e.g., [76–78]. Abrupt marine environmental changes are expected to become more common as climate change progresses [35]. Warming trends and/or abnormal temperature changes may affect the abundance, mortality, growth, and distribution of marine fish [33,34,79]. Here, we showed that the large fish assemblage in the ECS winter fishing ground in February and March 2017 may have been associated with abnormal temperature changes associated with the eastward movement of the YSCC. This event provided a rare case study that exemplified how complex relationships among climate-driven physical changes and biological processes may affect fishery resources. Future fishery management programs must develop strategies to adapt to similar environmental events that will become more frequent due to climate change.

5. Conclusions

Large fish assemblages were reported in the winter fishing grounds of the ECS during February and March 2017. The bottom waters of these fishing grounds were abnormally warm in winter 2017. This layer then cooled substantially from January to mid-March 2017 due to the eastward movement of the YSCC associated with the increased northwesterly winds. Warm-temperature demersal fish, such as the small yellow croaker (*Larimichthys polyactis*) and *Collichthys sp.*, might tend to migrate to fishing areas with warm temperature, strong thermal front, and high Chl *a* concentrations; these conditions were found in fishing areas Nos. 1891 and 1592 during February and March 2017. The observed abnormal temperature changes in winter and early spring 2017 might reflect the effects of changes in local ocean circulation.

This preliminary study proposes some possible mechanisms underlying the formation of two large fish assemblages based on satellite remote sensing and reanalysis data. Long-term time series data, obtained using a variety of coastal ocean observing systems [80], in conjunction with numerical models, are required to clarify and explain these physical mechanisms further. However, this rare case study demonstrates how fishery resources respond to climate-driven physical and biological changes. Thus, fishery management programs should carefully consider ecological responses to similar abnormal changes in marine environment.

Author Contributions: Conceptualization, C.Z. and W.D.; methodology, C.Z.; validation, W.D. and C.Z.; formal analysis, C.Z. and W.D.; investigation, W.D.; resources, C.Z. and W.D.; data curation, W.D.; writing—original draft preparation, W.D.; writing—review and editing, C.Z., W.D., J.H. and S.S.; visualization, W.D.; supervision, C.Z.; project administration, C.Z.; funding acquisition, C.Z. All authors have read and agreed to the published version of the manuscript.

Funding: This research was funded by the Key Program of NSF-China (NSFC) (Grant No. U1805241) and the National Key Research and Development Plan of China (Grant Nos. 2016YFE0202100, 2018YFC1406302).

Data Availability Statement: Publicly available data sets were analyzed in this study. OSTIA and ARMOR3D data were downloaded from Europe Copernicus program (<http://marine.copernicus.eu>, accessed on 2 March 2021). ASCAT wind and MODIS ocean color data were produced by Remote Sensing Systems (<http://www.remss.com>, accessed on 2 March 2021) and NASA Goddard Space Flight Center (<https://oceancolor.gsfc.nasa.gov>, accessed on 2 March 2021), respectively. VIIRS DNB radiance data were downloaded from the Earth Observations Group (<https://payneinstitute.mines.edu/eog/nighttime-lights/>, accessed on 2 March 2021). Himawari-8 Chl a concentration were downloaded from the P-Tree System (<https://www.eorc.jaxa.jp/ptree/index.html>, accessed on 2 March 2021).

Acknowledgments: Anonymous reviewers contributed substantially to the improvement of this paper.

Conflicts of Interest: The authors declare no conflict of interest.

References

1. Lie, H.-J.; Cho, C.-H. Recent advances in understanding the circulation and hydrography of the East China Sea. *Fish. Oceanogr.* **2002**, *11*, 318–328, doi:10.1046/j.1365-2419.2002.00215.x.
2. Drinkwater, K.F.; Tremblay, M.J.; Comeau, M. The influence of wind and temperature on the catch rate of the American lobster (*Homarus americanus*) during spring fisheries off eastern Canada. *Fish. Oceanogr.* **2006**, *15*, 150–165, doi:10.1111/j.1365-2419.2005.00349.x.
3. Winters, D.B. Offshore Wind Energy Impacts on Fisheries: Investigating Uncharted Waters in Research and Monitoring. *Fisheries* **2018**, *43*, 343–344, doi:10.1002/fsh.10126.
4. Mills, K.E.; Pershing, A.J.; Brown, C.J.; Chen, Y.; Chiang, F.-S.; Holland, D.S.; Lehuta, S.; Nye, J.A.; Sun, J.C.; Thomas, A.C.; et al. Fisheries Management in a Changing Climate: Lessons From the 2012 Ocean Heat Wave in the Northwest Atlantic. *Oceanography* **2013**, *26*, 191–195, doi:10.5670/oceanog.2013.27.
5. Sambou, O.S.; Kang, B.; Xu, H.X.; Zhou, Y.D.; Panhwar, S.K. Fish assemblage in the Hairtail Protected Area, East China Sea in relation to environmental variables. *Cah. Biol. Mar.* **2020**, *61*, 279–289, doi:10.21411/CBM.A.BADEE218.
6. Huang, M.R.; Ding, L.Y.; Wang, J.; Ding, C.Z.; Tao, J. The impacts of climate change on fish growth: A summary of conducted studies and current knowledge. *Ecol. Indic.* **2021**, *121*, 106976.
7. Xu, Z.L.; Chen, J.J. Analysis on migratory routine of *Larimichthys polyactis*. *J. Fish. Sci. China* **2009**, *16*, 931–940.
8. Eveson, J.P.; Hobday, A.J.; Hartog, J.R.; Spillman, C.M.; Rough, K.M. Seasonal forecasting of tuna habitat in the Great Australian Bight. *Fish. Res.* **2015**, *170*, 39–49, doi:10.1016/j.fishres.2015.05.008.
9. Methven, D.A.; Piatt, J.F. Seasonal abundance and vertical distribution of capelin (*Mallotus villosus*) in relation to water temperature at a coastal site off eastern Newfoundland. *ICES J. Mar. Sci.* **1991**, *48*, 187–193, doi:10.1093/icesjms/48.2.187.
10. Chang, Y.; Lee, M.-A.; Lee, K.-T.; Shao, K.-T. Adaptation of fisheries and mariculture management to extreme oceanic environmental changes and climate variability in Taiwan. *Mar. Policy* **2013**, *38*, 476–482, doi:10.1016/j.marpol.2012.08.002.
11. Hu, X.M.; Xiong, X.J.; Qiao, F.L.; Guo, B.H.; Lin, X.P. Surface current field and seasonal variability in the Kuroshio and adjacent regions derived from satellite-tracked drifter data. *Acta Oceanol. Sin.* **2008**, *27*, 11–29.
12. Zuo, J.; Song, J.; Yuan, H.; Li, X.; Li, N.; Duan, L. Impact of Kuroshio on the dissolved oxygen in the East China Sea region. *J. Oceanol. Limnol.* **2018**, *37*, 513–524, doi:10.1007/s00343-019-7389-5.
13. Yang, X.M.; Yao, T.D. The progress on the Asian monsoon study. *Chin. J. Nat.* **1999**, *6*, 3–5.
14. Ichikawa, H.; Beardsley, R.C. The Current System in the Yellow and East China Seas. *J. Oceanogr.* **2002**, *58*, 77–92, doi:10.1023/a:1015876701363.
15. Park, S.; Chu, P.C. Thermal and haline fronts in the Yellow/East China Seas: Surface and subsurface seasonality comparison. *J. Oceanogr.* **2006**, *62*, 617–638.
16. Chen, C.T.A. Chemical and physical fronts in the Bohai, Yellow and East China seas. *J. Mar. Syst.* **2009**, *78*, 394–410.
17. He, S.; Huang, D.; Zeng, D. Double SST fronts observed from MODIS data in the East China Sea off the Zhejiang–Fujian coast, China. *J. Mar. Syst.* **2016**, *154*, 93–102, doi:10.1016/j.jmarsys.2015.02.009.

18. Chang, Y.; Lee, M.A.; Shimada, T.; Sakaida, F.; Kawamura, H.; Chan, J.W.; Lu, H.J. Wintertime high-resolution features of sea surface temperature and chlorophyll-a fields associated with oceanic fronts in the southern East China Sea. *Int. J. Remote Sens.* **2008**, *29*, 6249–6261.
19. Huang, D.; Zhang, T.; Zhou, F. Sea-surface temperature fronts in the Yellow and East China Seas from TRMM microwave imager data. *Deep. Sea Res. Part II Top. Stud. Oceanogr.* **2010**, *57*, 1017–1024, doi:10.1016/j.dsr2.2010.02.003.
20. Zhao, C.Y. *Marine Fishery Resource of China*; Zhejiang Science and Technology Press: Hangzhou, China, 1990. (In Chinese)
21. Zheng, J.Y.; Chen, X.Z.; Cheng, J.H. *Fisheries Resource and Environment of Continental Shelf in East China Sea*; Shanghai Science and Technology Press: Shanghai, China, 2003. (In Chinese)
22. Cheng, J.; Cheung, W.W.; Pitcher, T.J. Mass-balance ecosystem model of the East China Sea. *Prog. Nat. Sci.* **2009**, *19*, 1271–1280.
23. Kang, J.-S. Analysis on the development trends of capture fisheries in North-East Asia and the policy and management implications for regional co-operation. *Ocean Coast. Manag.* **2006**, *49*, 42–67, doi:10.1016/j.ocecoaman.2005.10.002.
24. Zheng, B.; Chen, X.J.; Li, G. Relationship between the resource and fishing ground of mackerel and environmental factors based on GAM and GLM models in the East China Sea and Yellow Sea. *J. Fish. China* **2008**, *32*, 379–386.
25. Li, G.; Chen, X.; Lei, L.; Guan, W. Distribution of hotspots of chub mackerel based on remote-sensing data in coastal waters of China. *Int. J. Remote. Sens.* **2014**, *35*, 4399–4421, doi:10.1080/01431161.2014.916057.
26. Lin, H.-Y.; Chiu, M.-Y.; Shih, Y.-M.; Chen, I.-S.; Lee, M.-A.; Shao, K.-T. Species composition and assemblages of ichthyoplankton during summer in the East China Sea. *Cont. Shelf Res.* **2016**, *126*, 64–78, doi:10.1016/j.csr.2016.07.016.
27. Liu, K.-K.; Chao, S.-Y.; Lee, H.-J.; Gong, G.-C.; Teng, Y.-C. Seasonal variation of primary productivity in the East China Sea: A numerical study based on coupled physical-biogeochemical model. *Deep. Sea Res. Part II Top. Stud. Oceanogr.* **2010**, *57*, 1762–1782, doi:10.1016/j.dsr2.2010.04.003.
28. Zhang, C.-L.; Seo, Y.-I.; Kang, H.-J.; Lim, J.-H. Exploitable carrying capacity and potential biomass yield of sectors in the East China Sea, Yellow Sea, and East Sea/Sea of Japan large marine ecosystems. *Deep. Sea Res. Part II Top. Stud. Oceanogr.* **2019**, *163*, 16–28, doi:10.1016/j.dsr2.2018.11.016.
29. Teh, L.S.L.; Cashion, T.; Cheung, W.W.L.; Sumaila, U.R. Taking stock: A Large Marine Ecosystem perspective of socio-economic and ecological trends in East China Sea fisheries. *Rev. Fish Biol. Fish.* **2020**, *30*, 269–292, doi:10.1007/s11160-020-09599-8.
30. Jiang, Y.Z.; Cheng, J.H.; Li, S.F. Temporal changes in the fish community resulting from a summer fishing moratorium in the northern East China Sea. *Mar. Ecol. Prog. Ser.* **2009**, *387*, 265–273.
31. Chen, W.Z.; Zheng, Y.Z.; Chen, Y.Q.; Mathews, C.P. An assessment of fishery yields from the East China Sea Ecosystem. *Mar. Fish. Rev.* **1997**, *59*, 1–7.
32. FAO. *The State of World Fisheries and Aquaculture*; FAO: Rome, Italy, 1997; p. 125.
33. Edwards, M.; Richardson, A.J. Impact of climate change on marine pelagic phenology and trophic mismatch. *Nat. Cell Biol.* **2004**, *430*, 881–884, doi:10.1038/nature02808.
34. Perry, A.L.; Low, P.J.; Ellis, J.R.; Reynolds, J.D. Climate Change and Distribution Shifts in Marine Fishes. *Science* **2005**, *308*, 1912–1915, doi:10.1126/science.1111322.
35. Tebaldi, C.; Hayhoe, K.; Arblaster, J.M.; Meehl, G.A. Going to the Extremes. *Clim. Chang.* **2006**, *79*, 185–211, doi:10.1007/s10584-006-9051-4.
36. Sukgeun, J.; Hyung, K.C. Fishing vs. Climate Change: An example of filefish (*Thamnaconus modestus*) in the northern east China sea. *J. Mar. Sci. Technol.* **2013**, *21*, 15–22, doi:10.6119/JMST-013-1219-3.
37. Wall, C.C.; Muller-Karger, F.E.; Roffer, M.A.; Hu, C.; Yao, W.; Luther, M.E. Satellite remote sensing of surface oceanic fronts in coastal waters off west-central Florida. *Remote. Sens. Environ.* **2008**, *112*, 2963–2976, doi:10.1016/j.rse.2008.02.007.
38. Straka, W.; Seaman, C.J.; Baugh, K.; Cole, K.; Stevens, E.; Miller, S.D. Utilization of the Suomi National Polar-Orbiting Partnership (NPP) Visible Infrared Imaging Radiometer Suite (VIIRS) Day/Night Band for Arctic Ship Tracking and Fisheries Management. *Remote. Sens.* **2015**, *7*, 971–989, doi:10.3390/rs70100971.
39. Cozzolino, E.; Lasta, C.A. Use of VIIRS DNB satellite images to detect jigger ships involved in the *Illex argentinus* fishery. *Remote. Sens. Appl. Soc. Environ.* **2016**, *4*, 167–178, doi:10.1016/j.rsase.2016.09.002.
40. Waluda, C.M.; Griffiths, H.J.; Rodhouse, P.G. Remotely sensed spatial dynamics of the *Illex argentinus* fishery, Southwest Atlantic. *Fish. Res.* **2008**, *91*, 196–202.
41. Cooke, S.; Lennox, R.; Bower, S.; Horodysky, A.; Trembl, M.; Stoddard, E.; Donaldson, L.; Danylchuk, A. Fishing in the dark: The science and management of recreational fisheries at night. *Bull. Mar. Sci.* **2017**, *93*, 519–538, doi:10.5343/bms.2015.1103.
42. Hammerschlag, N.; Meyer, C.; Grace, M.; Kessel, S.; Sutton, T.; Harvey, E.; Paris-Limouzy, C.; Kerstetter, D.; Cooke, S. Shining a light on fish at night: An overview of fish and fisheries in the dark of night, and in deep and polar seas. *Bull. Mar. Sci.* **2017**, *93*, 253–284, doi:10.5343/bms.2016.1082.
43. Elvidge, C.D.; Baugh, K.; Zhizhin, M.; Hsu, F.C.; Ghosh, T. VIIRS night-time lights. *Int. J. Remote. Sens.* **2017**, *38*, 5860–5879, doi:10.1080/01431161.2017.1342050.
44. Mulet, S.; Rio, M.-H.; Mignot, A.; Guinehut, S.; Morrow, R. A new estimate of the global 3D geostrophic ocean circulation based on satellite data and in-situ measurements. *Deep. Sea Res. Part II Top. Stud. Oceanogr.* **2012**, *77–80*, 70–81, doi:10.1016/j.dsr2.2012.04.012.
45. Guinehut, S.; Dhomp, A.-L.; Larnicol, G.; Le Traon, P.-Y. High resolution 3-D temperature and salinity fields derived from in situ and satellite observations. *Ocean Sci.* **2012**, *8*, 845–857, doi:10.5194/os-8-845-2012.

46. Kim, S.H.; Choi, B.K.; Kim, E. Study on the Behavior of the Water Temperature Inversion Layer in the Northern East China Sea. *J. Mar. Sci. Eng.* **2020**, *8*, 157, doi:10.3390/jmse8030157.
47. Solomon, O.O.; Ahmed, O.O. Fishing with light: Ecological consequences for coastal habitats. *Int. J. Fish. Aquat. Stud.* **2016**, *4*, 474–483.
48. Du, J.-L.; Yang, S.-L.; Feng, H. Recent human impacts on the morphological evolution of the Yangtze River delta foreland: A review and new perspectives. *Estuarine, Coast. Shelf Sci.* **2016**, *181*, 160–169, doi:10.1016/j.ecss.2016.08.025.
49. Lin, L.; Liu, Z.; Jiang, Y.; Huang, W.; Gao, T. Current status of small yellow croaker resources in the southern Yellow Sea and the East China Sea. *Chin. J. Oceanol. Limnol.* **2011**, *29*, 547–555, doi:10.1007/s00343-011-0182-8.
50. Chen, J.-J.; Xu, Z.-L.; Chen, X.-Z. The spatial distribution pattern of fishing ground for small yellow croaker in China Seas. *J. Fish. China* **2010**, *34*, 236–244, doi:10.3724/sp.j.1231.2010.06371.
51. Liu, X. *The Research of Small Yellow Croaker (Larimichthys polyactis) Geographic Race and Gonad*; Science Press: Beijing, China, 1962; pp. 35–70.
52. Li, X.D. A preliminary study on the division of water-system and fishing grounds during winter in the south of Huanghai Sea and the East China Sea. *Mar. Forecast. Serv.* **1985**, *2*, 67–72.
53. Liu, Z.L.; Yuan, X.W.; Yang, L.L.; Yan, L.P.; Tian, Y.J.; Chen, J.H. Effect of climate change on the fisheries community pattern in the overwintering ground of open waters of northern East China Sea. *Chin. J. Appl. Ecol.* **2015**, *26*, 901–911, doi:10.13287/j.1001-9332.20150106.013.
54. Xu, Z.L.; Wang, R.; Chen, Y.Q. Study on ecology of meso-small pelagic copepods in the Southern Yellow Sea and the East China Sea I. Quantitative distribution. *J. Fish. China* **2003**, *27*, 1–8, doi:10.3321/j.issn:1000-0615.2003.z1.001.
55. Yatsu, A.; Watanabe, T.; Ishida, M.; Sugisaki, H.; Jacobson, L.D. Environmental effects on recruitment and productivity of Japanese sardine *Sardinops melanostictus* and chub mackerel *Scomber japonicus* with recommendations for management. *Fish. Oceanogr.* **2005**, *14*, 263–278, doi:10.1111/j.1365-2419.2005.00335.x.
56. Yukami, R.; Ohshimo, S.; Yoda, M.; Hiyama, Y. Estimation of the spawning grounds of chub mackerel *Scomber japonicus* and spotted mackerel *Scomber australasicus* in the East China Sea based on catch statistics and biometric data. *Fish. Sci.* **2009**, *75*, 167–174, doi:10.1007/s12562-008-0015-7.
57. Guo, A.; Yu, W.; Chen, X.J.; Qian, W.G.; Li, R.C. Relationship between spatio-temporal distribution of chub mackerel *Scomber japonicus* and net primary production in the coastal waters of China. *Acta Oceanol. Sin.* **2018**, *40*, 42–52, doi:10.3969/j.issn.0253-4193.2018.08.005.
58. Liu, F.; Chu, T.; Wang, M.; Zhan, W.; Xie, Q.; Lou, B. Transcriptome analyses provide the first insight into the molecular basis of cold tolerance in *Larimichthys polyactis*. *J. Comp. Physiol. B* **2019**, *190*, 27–34, doi:10.1007/s00360-019-01247-3.
59. O’Gorman, E.J.; Ólafsson, Ólafur, P.; Demars, B.O.L.; Friberg, N.; Guðbergsson, G.; Hannesdóttir, E.R.; Jackson, M.C.; Johansson, L.S.; McLaughlin, Órla, B.; Ólafsson, J.S.; et al. Temperature effects on fish production across a natural thermal gradient. *Glob. Chang. Biol.* **2016**, *22*, 3206–3220, doi:10.1111/gcb.13233.
60. Friedland, K.D.; Langan, J.A.; Large, S.I.; Selden, R.L.; Link, J.S.; Watson, R.A.; Collie, J.S. Changes in higher trophic level productivity, diversity and niche space in a rapidly warming continental shelf ecosystem. *Sci. Total. Environ.* **2020**, *704*, 135270, doi:10.1016/j.scitotenv.2019.135270.
61. Moser, H.G.; Smith, P.E. Larval fish assemblages of the California Current region and their horizontal and vertical distributions across a front. *Bull. Mar. Sci.* **1993**, *53*, 645–691.
62. Sournia, A. Pelagic biogeography and fronts. *Prog. Oceanogr.* **1994**, *34*, 109–120, doi:10.1016/0079-6611(94)90004-3.
63. Okazaki, Y.; Nakata, H. Effect of the mesoscale hydrographic features on larval fish distribution across the shelf break of East China Sea. *Cont. Shelf Res.* **2007**, *27*, 1616–1628, doi:10.1016/j.csr.2007.01.024.
64. Bost, C.; Cotté, C.; Bailleul, F.; Cherel, Y.; Charrassin, J.; Guinet, C.; Ainley, D.; Weimerskirch, H. The importance of oceanographic fronts to marine birds and mammals of the southern oceans. *J. Mar. Syst.* **2009**, *78*, 363–376, doi:10.1016/j.jmarsys.2008.11.022.
65. Kindong, R.; Wu, J.; Gao, C.; Dai, L.; Tian, S.; Dai, X.; Chen, J. Seasonal changes in fish diversity, density, biomass, and assemblage alongside environmental variables in the Yangtze River Estuary. *Environ. Sci. Pollut. Res.* **2020**, *27*, 25461–25474, doi:10.1007/s11356-020-08674-8.
66. Yeh, S.W.; Kim, C.H. Recent warming in the yellow/East China Sea during winter and the associated atmospheric circulation. *Cont. Shelf Res.* **2010**, *30*, 1428–1434.
67. Cai, R.; Tan, H.; Kontoyiannis, H. Robust surface warming in offshore China seas and its relationship to the east Asian monsoon wind field and ocean forcing on interdecadal time scales. *J. Clim.* **2017**, *30*, 8987–9005.
68. Cai, R.; Tan, H.; Qi, Q. Impacts of and adaptation to inter-decadal marine climate change in coastal China seas. *Int. J. Clim.* **2015**, *36*, 3770–3780, doi:10.1002/joc.4591.
69. Qi, L.; Hu, C.; Wang, M.; Shang, S.; Wilson, C. Floating Algae Blooms in the East China Sea. *Geophys. Res. Lett.* **2017**, *44*, 11–501, doi:10.1002/2017gl075525.
70. Su, J.L. A review of circulation dynamics of the coastal oceans near China. *Acta Oceanol. Sin.* **2001**, *4*, 1–16.
71. Guan, B.; Fang, G. Winter counter-wind currents off the southeastern China coast: A review. *J. Oceanogr.* **2006**, *62*, 1–24, doi:10.1007/s10872-006-0028-8.
72. Weisberg, R.H.; Zheng, L.; Liu, Y. Basic tenets for coastal ocean ecosystems monitoring. In *Coastal Ocean Observing Systems*; Academic Press: Cambridge, MA, USA, 2015; pp. 40–57, doi:10.1016/b978-0-12-802022-7.00004-3.

73. IPCC. *Climate Change 2007: The Physical Science Basis, Contribution of Working Group I to the Fourth Assessment Report of the Intergovernmental Panel on Climate Change*; Solomon, S., Qin, D., Manning, M., Chen, Z., Marquis, M., Averyt, K.B., Tignor, M., Miller, H.L., Eds.; Cambridge University Press: New York, NY, USA, 2007.
74. Strüssmann, C.A.; Conover, D.O.; Somoza, G.M.; Miranda, L.A. Implications of climate change for the reproductive capacity and survival of New World silversides (family Atherinopsidae). *J. Fish Biol.* **2010**, *77*, 1818–1834, doi:10.1111/j.1095-8649.2010.02780.x.
75. Brander, K.M. Cod *Gadus morhua* and climate change: Processes, productivity and prediction. *J. Fish Biol.* **2010**, *77*, 1899–1911, doi:10.1111/j.1095-8649.2010.02782.x.
76. Belkin, I.M. Rapid warming of Large Marine Ecosystems. *Prog. Oceanogr.* **2009**, *81*, 207–213, doi:10.1016/j.pocean.2009.04.011.
77. Liu, Q.; Zhang, Q. Analysis on long-term change of sea surface temperature in the China Seas. *J. Ocean Univ. China* **2013**, *12*, 295–300, doi:10.1007/s11802-013-2172-2.
78. Bao, B.; Ren, G. Climatological characteristics and long-term change of SST over the marginal seas of China. *Cont. Shelf Res.* **2014**, *77*, 96–106, doi:10.1016/j.csr.2014.01.013.
79. Nye, J.; Link, J.; Hare, J.; Overholtz, W. Changing spatial distribution of fish stocks in relation to climate and population size on the Northeast United States continental shelf. *Mar. Ecol. Prog. Ser.* **2009**, *393*, 111–129, doi:10.3354/meps08220.
80. Liu, Y.G.; Kerkering, H.; Weisberg, R. *Coastal Ocean Observing Systems*; Academic Press: London, UK, 2015.